A Zero Index Based Meta-Lens Loaded Wideband Directive Antenna Combined With Reactive Impedance Surface

BASUDEV MAJUMDER[1], **KRISHNAMOORTHY KANDASAMY**[2],
AND KAMLA PRASAN RAY[3], **(Senior Member, IEEE)**

[1]Department of Avionics, Indian Institute of Space Science and Technology, Thiruvananthapuram 695547, India
[2]Department of Electronics and Communication Engineering, National Institute of Technology Karnataka, Mangalore 575025, India
[3]Electronics Engineering Department, Defense Institute of Advanced Technology, Pune 411025, India

Corresponding author: Basudev Majumder (bmbasudev30@gmail.com)

ABSTRACT In this paper, an aperture efficient wideband high-gain patch antenna is designed using a novel multilayer-based metamaterial structure combined with a reactive impedance surface (RIS)-backed patch antenna. The metamaterial unit cell is a two-layer structure which is stacked one after other to form the overall unit cell. The microscopic behavior of the proposed unit cell has been investigated. This unit cell gives low refractive index over a wide bandwidth with a negligible loss. An RIS-backed patch antenna has been designed in the required frequency band to feed the multilayer zero-index metamaterial medium. The introduction of this surface is to provide unidirectional radiation over a wideband in the zero refractive index region. The proposed antenna gives a 14% fractional bandwidth over the *C*- and *X*-bands. The proposed antenna enhances the peak gain of the conventional patch antenna by an amount of 8.5 dB at 8 GHz. Finally, the antenna has been fabricated and its performance is verified experimentally.

INDEX TERMS Reactive impedance surface (RIS), high gain, zero indexed metamaterial layer (ZIML).

I. INTRODUCTION

High gain wide band planar antennas have gained major attention because they can produce high gain across a wide operating bandwidth with low complexity using PCB technology. These types of antennas are very useful in wireless broadcasting and as an integral part of the radar systems. To increase the directivity of the planar antennas, Resonant Cavity Antennas (RCA) based on the Fabry–Pérot concept [1] has been proposed. In these antennas, a primary source is kept between two semi-transparent partially reflecting superstrates (PRS) separated by half a wave length. Since their inception, many transparent and semitransparent superstrates have been proposed to enhance the gain. In [2]–[4], a dielectric slab-based superstrate is proposed. In [5] and [6], frequency selective surfaces have been used to enhance the gain. A metallic grid-based PRS [7] has also been proposed to enhance the broadside directivity. Electromagnetic bandgap structures [8] and artificial magnetic conductors (AMCs) [9]–[12] have been used to focus the radiation and to improve the gain. In [13] and [14], a Mu near zero superstrate has been used to improve the directivity of the antenna.

Also using the metasurface based technology compact broadband directive antennas have been reported [15], [16]. Apart from this, many research groups have investigated the low index material or zero index material made up of subwavelength elements which work in the frequency range where either the extracted permittivity or the permeability or both of the medium is low. The electromagnetic wave travelling in these mediums encounter very less phase variation. This helps the electromagnetic energy to tunnel through the small cross sections of the irregular shape [17]. Cloaking [18] and lenses [19] are the two pioneering application of this phenomena. As the electromagnetic wave inside the low-index medium (LIM) freezes and cannot propagate, the outgoing wave from this medium show conformal and homogeneous phase front and according to the Snell's law the outgoing wave will bend towards the normal. Due to this property, ZIMs are very popular to focus the beam. Using this principle, in [20] the directivity of a line source embedded in a LIM/ZIM has been enhanced experimentally. In [21] the energy from a dipole antenna embedded in a ZIM has been concentrated around the surrounding media. In [22]

horn antennas gain has been enhanced by the use of the ZIM loading. In [23] an EBG backed dipole antennas gain has been enhanced using low index based 3D meta-material based superstrate. But, ttheir applications are limited because they are bulky and their fabrications are also complex as compared to the planar directive antennas. Recently, designing directive planar meta-material based antennas have become much popular [24]–[26] using ZIML based approach. But most of them have been used to enhance the gain within a very narrow bandwidth or provide less efficiency.

In this paper a multi-layer metamaterial based antenna is designed to produce high gain over the wide band. The proposed two layer medium are capable of providing low indexes over a wide band which is suitable for achieving the high directivity across the wide band. In [3] and [10] wide band high gain antennas are reported using a partially reflecting based superstrate fed by an aperture coupled microstrip antenna. But the drawback of the aperture coupled antennas are, they have poor front to back lobe ratio and poor radiation efficiency because of the presence of the slot at their back. So, to feed our wide band multilayer ZIML medium, a reactive impedance surface (RIS) backed patch antenna has been used. The proposed RIS backed antenna is designed within the frequency band of the zero indexed region of the multilayer layer metamaterial structure. The RIS, besides making the feed antenna compact, provides a wide-bandwidth by introducing an additional resonance and more uni-directional radiation over a wide-bandwidth as compared to other conventional planar low profile feeds. The antenna has been simulated in CST MWS [27] and the results have been verified experimentally.

II. GUIDELINES FOR DESIGNING UNIT CELL

A. DESIGNING ZIML BASED MULTILAYER UNIT CELL

The metamaterial (MM) unit cell considered as the superstrate of the antenna can be thought of as an array of asymmetric I shaped metallic thin wire whose period is equal to the one fourth of the operating wavelength. The inspiration of selecting this unit cell is physically explained in [28] and [29]. In [28] and [29] it was reported that the continuous thin wire can be characterized by the plasma frequency, $\varepsilon_{\text{eff}} = \varepsilon_0(1 - \omega_{\text{p}}^2/\omega^2)$ where ε_{eff} is the effective permittivity, ω_{p} is the plasma frequency and ω is the frequency of the incoming electromagnetic wave. The thin wires exhibit the zero refractive index where the operating frequency is closed to the plasma frequency. In the proposed design, the unit cell structure is printed on both the sides of a Rogers RT/ Duroid substrate having permittivity of 2.2 thickness of 0.787 mm and loss tangent of 0.001. The unit cell consists of two layers which are stacked one after other along the direction of the wave propagation as shown in Fig. 1(b). The front face of it is shown in Fig. 1(a).

The two layer structure is excited by the plane wave which is incident perpendicular to its plane and the four sides of the unit cell are set to have periodic boundary conditions (PBC).
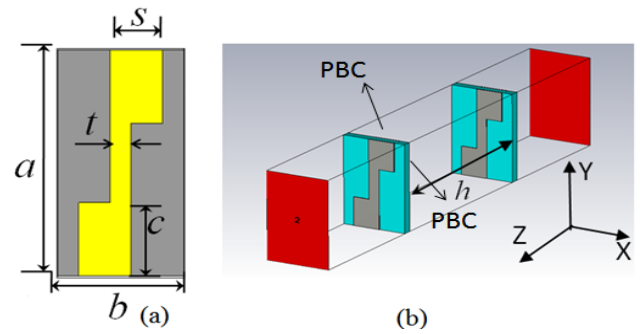

FIGURE 1. Superstrate unit cell (a) front view of the unit cell (b) multilayer unit cell.

The lateral dimension of the unit cell is set to have $a = 0.16\,\lambda_{\text{g}}$ and $b = 0.27\,\lambda_{\text{g}}$. λ_{g}, is defined as the equivalent operating wavelength inside the dielectric material. Characterization of the MM unit cell parameter is done from its scattering parameter results using the algorithm explained in [30]. Fig. 2 depicts the unit cell scattering response for perpendicular electromagnetic wave propagation. It shows that the unit cell resonates around 8 GHz and at this frequency transmission co-efficient becomes unity. Fig. 2 (b) shows that at the resonating frequency point the reflection phase point undergoes a phase change of 180°. Fig. 2(c) shows the surface current distribution on the unit cell element considering the electromagnetic wave at port 1. It reveals that at resonant condition the vertical arms of the unit cells contribute more to the resonance. That is why strong intensity of the surface current is observed around the vertical arms. The total thickness of the unit cell along the direction of the electromagnetic wave propagation is 0.4 times at the operating frequency which is at 8 GHz. This ensures that the incoming electromagnetic wave does not undergo local phase change within the material and the limit of the bulk homogenization property is not reached. So the extraction of the bulk medium parameters remains valid while using the algorithm [30]. Fig. 3 (a) examines the equivalent extracted material property of the proposed unit cell for the normal incidence of the incoming electromagnetic wave. From Fig. 3 (a) it is observed that the proposed unit cell has the extracted refractive index near to zero between the frequencies of 7.6 GHz, and 8.4 GHz and around 8 GHz the refractive index value becomes zero which is the point where the electromagnetic wave gets frozen. The imaginary part of the index curve is also observed below 0.7 over the bandwidth. Fig. 3(b) and (c) investigates the variation of the return loss and the extracted refractive index for different incident angles. From Fig. 3(b) it can be observed that as the incident angle increases the return loss plot shifts towards the higher frequency. Fig (c) shows that between 7.4 GHz and 8.5 GHz the real part of refractive index remains below 1 which is well within the working bandwidth limit ($|n| < 1$) of the ZIML structure for the different incident angles. It is also noted that within this bandwidth, imaginary part of the respective index curve (for different incident angles) is below 0.7 like the case of the normal incidence.
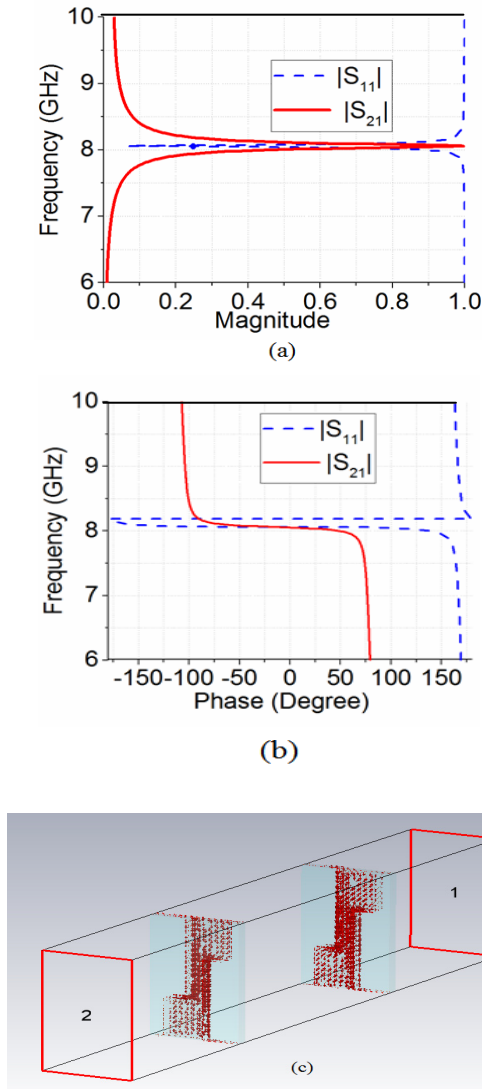
FIGURE 2. Scattering parameter response and surface current distribution of the proposed unit cell (a) Magnitude response (b) Phase response (c) surface current distribution at 8 GHz for incoming electromagnetic wave at port 1.

FIGURE 3. (a) Extracted Refractive Index using the Kramer Algorithm (b) variation of reflection co-efficient with incident angle. (c) Variation of the real part of the refractive index with the incident angle.

FIGURE 4. Dispersion Diagram of the unit cell (a) variation of TM modes over the frequency (b) zoomed version of Fig. (a).

With this information it can be inferred that the proposed two layer ZIM based unit cell can efficiently act as an artificial lens-like medium which can focus the incoming electromagnetic wave efficiently by bending the emitted wave towards its normal. The proposed ZIML based meta-lens has very low imaginary value close to zero which suggests that the meta-lens medium will be less lossy. It can be seen that the imaginary part of the refractive index value is positive which maintains the passivity and the causality property of this met-alens medium. The dispersion diagram plot in Fig. 4 further verifies the presence of the refractive index region. It has been plotted using CST Eigen mode solver to further verify the zero indexed region considering suitable boundary condition for the proposed periodicity value. Fig. 4 reveals that if the proposed unit cell is placed periodically, it will still act as a ZIML medium.
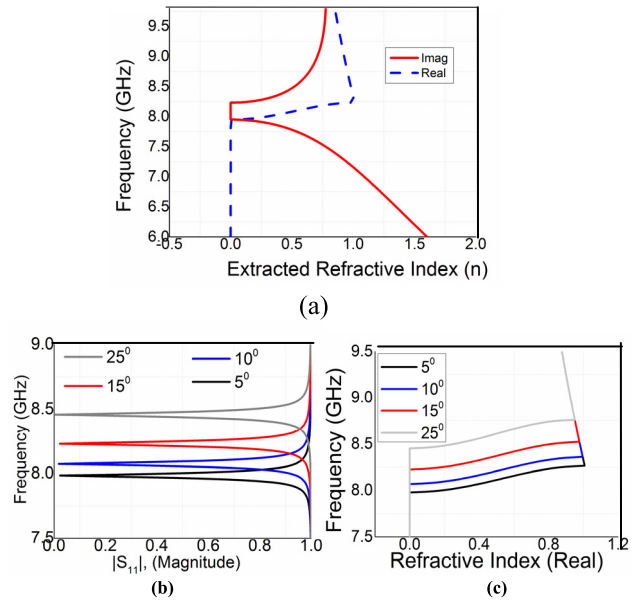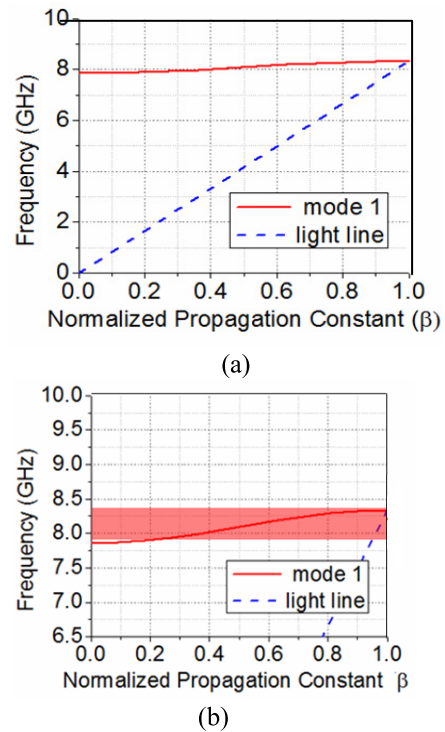
In order to make the overall profile of the antenna low, two-layer structure has been characterized and fabricated. Fig. 4 shows that between the frequencies 7.5 GHz and 8.5 GHz, the ratio of the velocity of the light at free space to its velocity in that medium which is nothing but the refractive

index, at that medium is less than one. So similar observation using this fact indirectly verifies the results obtained using Kramer Algorithm [30]. So, from our above discussion it is clear that the 6 X 6 of the proposed unit can be arranged periodically along the X and Y direction to form the metalens medium to improve the radiation from an incoming electromagnetic source.

B. DESIGNING PATCH TYPE RIS UNIT CELL

To feed the proposed metalens medium a RIS backed patch antenna is designed. The introduction of the RIS surface is to obtain the compact and wide band behavior and more unidirectional response from the conventional narrow band patch antenna. For designing this surface conventional square patch type unit cell is chosen. The RIS surface consists of a 6 X 6 metallic patch type elements which are arranged periodically along both the X and Y directions. The unit cell is shown in Fig. 5(a). These elements are printed on a substrate having permittivity of 2.2 thickness of 1 mm and loss tangent of 0.001. The dimensions of this unit cell element along with the ZIM unit cell are given in Table 1. The variation of the reflection phase over the frequency band of the proposed unit cell is shown in Fig 5 (c). It is observed

that the reflection phase curve crosses the zero at 8.15 GHz. The reflection phase curve can vary between $+90°$ and $-90°$ in the frequencies of 7.4 GHz and 9.3 GHz. The reflection phase characteristics of RIS patches is invariant with respect to the incident angle. To get a wide band feed, a patch antenna backed by an RIS surface is proposed. The reflection phase surface has been optimized to get the unidirectional radiation pattern over a wide band. The working principal and the radiation mechanism of the proposed antenna and its experimental results have been described in the subsequent section.

III. ANTENNA DESIGN AND ITS WORKING PRINCIPLE

The zero index based multilayer superstrate tends to refract off-normal rays back towards the normal which is already shown in Fig. 3(c). The zero-index slab serves for maintaining an uniform and flat phase front across the surface of the superstrate layer due to its infinite effective phase velocity. It increases the overall aperture efficiency of the antenna. The metamaterial superstrate described in the last section has been fed by an RIS surface backed patch antenna operating at 7.8 GHz to enhance its forward radiation characteristics. The length of the RIS backed patch antenna is 10 mm and the width is set to 5.25 mm. Proper phase of the RIS surface over the bandwidth not only ensures compact operation as well as cancels the reactance of the patch antenna which gives rise to a wide band operation over the wide bandwidth This surface also helps to improve the radiation pattern of the feed pact antenna because of its in phase reflection behaviour around a narrow bandwidth of 8 GHz. The patch antenna is designed on a Rogers's RT/ Duroid substrate having permittivity of 2.2 and thickness of 0.787 mm. The ground plane area of the RIS backed antenna is 60 mm X 60 mm.
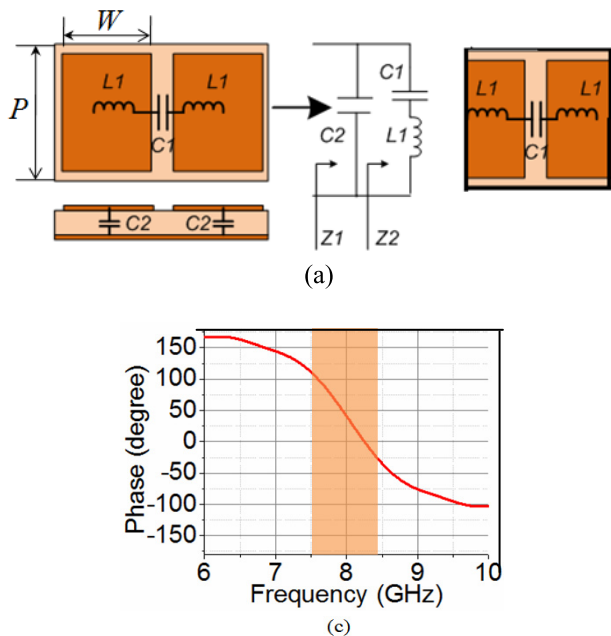

(a)

(c)

FIGURE 5. Description of the Reactive Impedance Surface (a) RIS unit cell (b) Circuit model of the equivalent RIS unit cell (c) Reflection Phase response.

TABLE 1. Optimized dimensions of the proposed RIS and ZIM unit cell.

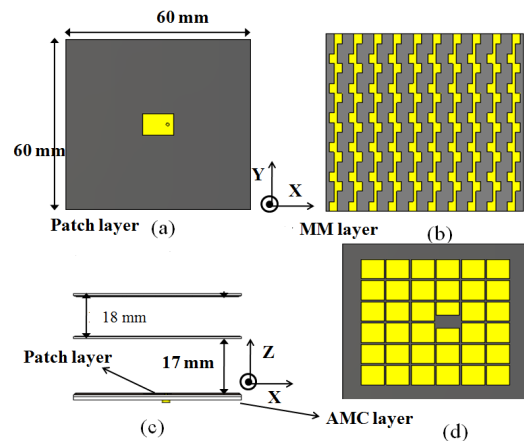| Parameter	P	W	a	B	C	t	s	h
Value (mm)	8.2	7.7	6	10	3.25	1	2.5	16.5

FIGURE 6. (a) Feed patch antenna (b) MM superstrate (c) side view of the antenna (d) RIS layer.

To be precise, the dimension of the RIS unit cell has been optimized in such a way so that the capacitive impedance of the patch antenna gets compensated by the inductive region of the phase response provided by the RIS surface. Fig. 6. presents the different layers of the proposed antenna. The superstrate layer consists of a 10 X 6 unit cells arranged
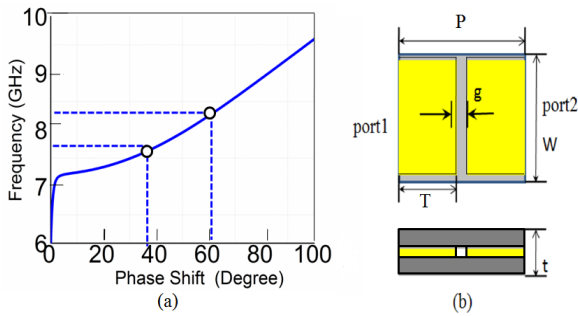
FIGURE 7. (a) Dispersion Diagram (b) Unit Cell.

periodically along both the X and Y directions as shown in Fig. 6(b). While designing the feed patch layer, the most sensitive parameters are the RIS unit cell width, inter-element spacing, patch length and the port position. These parameters can be optimized to get a wideband response. The spacing between the superstrate layer and the antenna should be optimized to get high gain and good impedance matching across the wide band. The loaded superstrate should not reflect and electromagnetic wave back to feed patch antenna since it can alter the transformed at the port. These dimensions majorly guide the resonance of the proposed antenna. Fig. 6(c) shows the side view of the simulated prototype. Optimized height between the feed layer and the MM based superstrate layer is obtained around 17 mm for which the antenna provides high gain over a wide bandwidth. The radiation mechanism and the resonating modes of the overall antenna can be visualized from Fig. 7. The thin metallic patch on the RIS surface acts as an excitation source for the RIS layer located below. The layer below when gets excited radiates through the gap of each patches consisting the RIS surface. From Fig. 7(a) it can be seen that at the frequency, 7.7 GHz, the angular phase shift from the RIS surface becomes around 36° for one-unit cell so for total 5 unit cell the combined phase shift becomes 180° causing the resonance. As a result of which the RIS matrix becomes responsible for providing the additional TM_{10} mode. Hence, patch type of radiation pattern is obtained. This phenomenon has further been justified by the electric field distribution in the RIS cavity in both the X and the Y direction. In the YZ plane no variation of the electric field is observed as shown in Fig. 8 (b) whereas in the XZ plane half wavelength variation is observed as shown in Fig. 8(a). Next, when the number of the unit cell is reduced to 3, the right resonance produced by it shifted to around 8.4 GHz (depicted in Fig. 8(e)), since the phase shift per-unit cell becomes 60° as depicted in Fig. 7(a). Since the lower resonance causes because of the feed patch antenna which becomes compact due to the inductive effect of the reflection phase of the RIS surface remains same. So, the RIS can create an additional resonance which can be shifted to merge with the actual resonance of the patch antenna. These two resonances help to achieve wide −10 dB impedance bandwidth (7.2 GHz – 8.2 GHz) as shown in Fig 8(e). Owing to the existence of the gaps between the RIS patches the quality
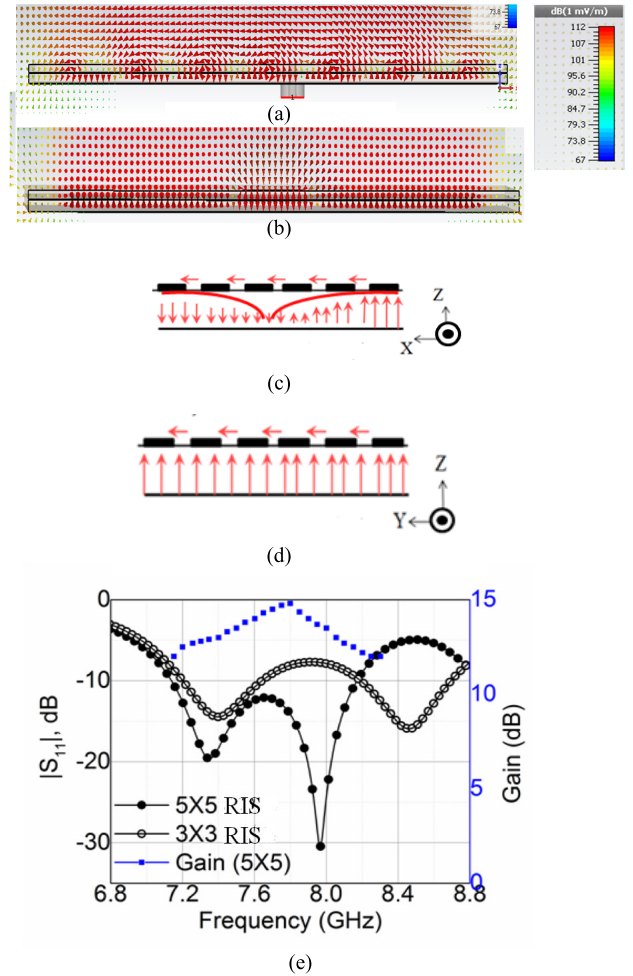

FIGURE 8. (a) Electric field variation in X direction (b) E filed Variation in Y direction (c) schematics of (a) (d) schematics of (b) (e) simulated input reflection co-efficient and gain plot.

factor of the antenna reduces which leads to the enhancement of the impedance bandwidth further. Also the presence of the gaps contributes to more fringing field which in-turn enhances the radiation efficiency and the gain of the overall antenna. It is noted that the gap (g) of the RIS unit cell changes both the dispersion property and the RIS bandwidth of the entire RIS simultaneously. Hence, both the resonating frequency changes their position. So the initial challenge is to design a radiation efficient broadband feed antenna which can excite the proposed ZIML layer which.

IV. ANTENNA FABRICATION AND ITS MEASUREMENT RESULTS

To test the antenna performance, a prototype is fabricated. The RIS and the patch both are printed on a Rogers substrate of permittivity 2.2 and thickness of 1 mm. The ZIML based metalens is printed on a Rogers substrate having permittivity 2.2 and thickness of 0.787 mm. The simulated −10 dB impedance bandwidth of the overall antenna is obtained from 7.21 GHz to 8.2 GHz, while the measured impedance

bandwidth is observed between 7.2 GHz and 8.15 GHz as shown in Fig. 10. The slight difference observed in the reflection co-efficient may arise from the inhomogeneous epsilon of the material or from the welded SMA connector.
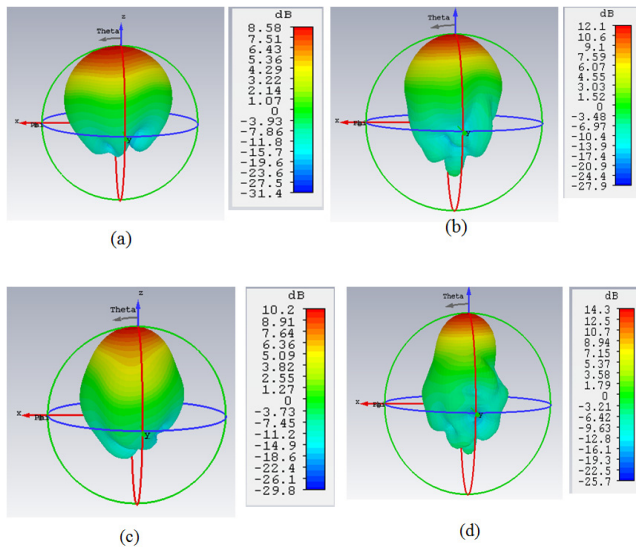

FIGURE 9. (a) 3D Radiation pattern (a) without RIS surface at 7.2 GHz (b) with RIS surface at 7.2 GHz. (c) without RIS surface at 8 GHz (d) with RIS surface at 8 GHz.

As the input impedance of the patch is sensitive to the height of the superstrate layer, further optimization is needed to get high gain response over the wide band. This optimized height selection is very important, since the zero-index meta-material slab helps the electromagnetic energy to concentrate to produce a plane wave which results in an increased directivity. Fabricated prototype has been characterized in a reflection free environment with the help of a standard transmitting horn operating at the same frequency band and a calibrated Vector Network Analyzer (VNA). At first the prototype has been placed in the far field of the transmitting horn and mounted on a positioned that can be rotated freely. After that the antenna is rotated in its two principal planes with respect to the co-polarized axis of the transmitting horn to obtain its co-polarized radiation pattern. Similarly, to measure the cross polarized pattern, the test antenna is placed at the cross fashion with respect to the transmitting horn so that the reception happened minimum. In this process one port of the VNA is connected to the transmitting horn and the other port is connected to the test antenna. The simulated and measured radiation patterns at both the principal planes has been achieve using the RIS based metasurface loading technique. To gain a better understanding of how the ZIML layer improves he radiation pattern, the 3D plot of the radiation pattern for with and without superstrate has been shown in Fig. 9. The loading of the ZIML layer enhances the gain around 4-5 dBi. It can be noted that the choice of feed could have been ordinary aperture coupled antenna, but it would drastically reduce the antenna front to back-lobe power. Hence the efficiency would have been low.
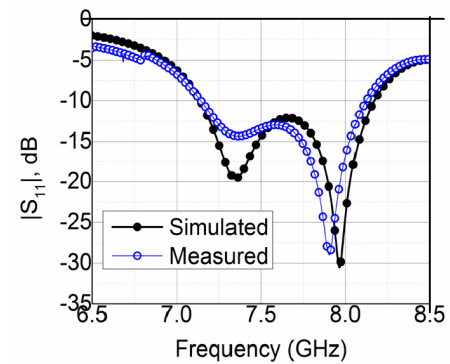

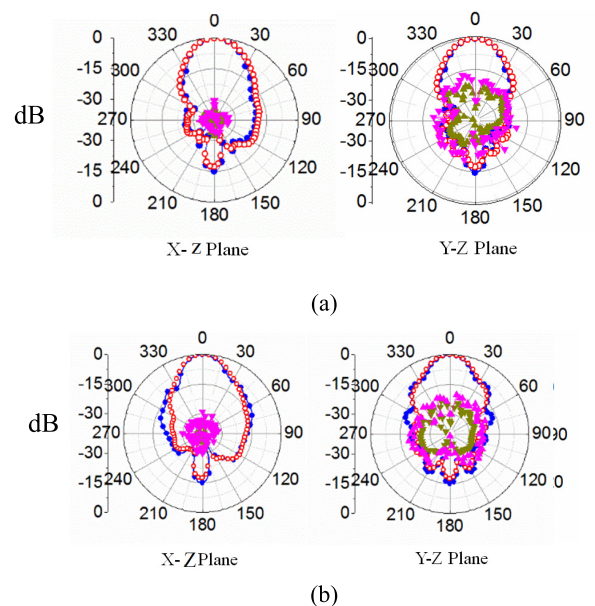**FIGURE 10.** Simulated and measured reflection co-efficient of the antenna.

FIGURE 11. Simulated and Measured Radiation Patterns of the proposed antenna. (a) at 7.8 GHz, (b) 8.2 GHz. [Red color: Co-pole meas, Blue color: Co-pole sim, Pink color: Cross-pole meas, Dark yellow color: Cross-pole simulated].

For our proposed over-all antenna, the FTBR is observed to be around 18 dB.are compared in Fig 11(a) and Fig 11(b). The measured results show good agreement with the simulated results, in both the principal planes. It is also observed that in the XZ plane the cross polarization level is 10 dB more as compared to the YZ plane. In the XZ plane, the cross-polarization level is obtained below −30 dB. But in the YZ. plane the cross-polarization level is obtained below −20 dB. The maximum simulated realized gain is obtained around 14.8 dBi at 7.9 GHz. The average simulated efficiency of the antenna over the band is around 90%-96%. The simulated efficiency of the proposed RIS backed meta-lens loaded patch antenna is observed around 94% at the frequency where gain is maximum. The simulated 3 dB beam-width in the H plane and E plane are 29° and 30°, respectively at the frequency where the maximum gain is observed. In both the principal planes the side lobe levels are down by −13 dB at 7.7 GHz.
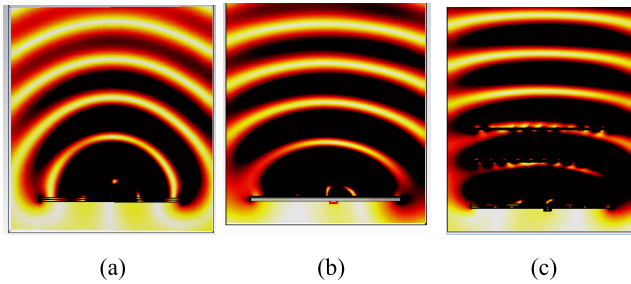
FIGURE 12. Electric field distribution at XZ Plane at 8 GHz.
(a) conventional patch antenna (b) RIS backed patch antenna
(c) ZIML loaded RIS backed patch antenna.

FIGURE 13. Electric field distribution at XY plane at 8 GHz.
(a) conventional patch antenna (b) RIS backed patch antenna
(c) ZIML loaded RIS backed patch antenna.
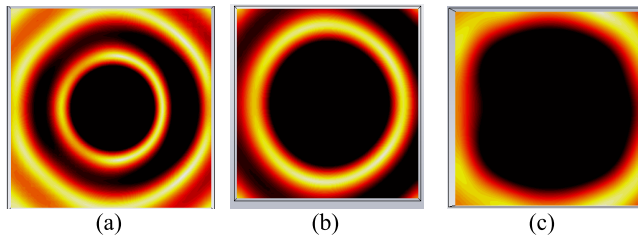
In order to investigate the improved performance of the RIS backed patch antenna further, the electric field distributions at two different principal planes are presented at 8 GHz in Fig. 12 and Fig. 13 with and without the RIS and meta-lens layer. From Fig. 12 it is clear that the wave-front of the electric field distribution leaving the ZIML layer becomes more uniform and planar instead of having spherical wave-front like conventional patch antenna case as shown in Fig. 12 (a). This planar wave-front justifies that the gain is significantly increased. It is also noted (from Fig. 12 (b)) that only with the RIS surface the gain of the patch antenna increases about 2.5-3 dB over the band.So the wave-front is seen to be planar than the conventional one but lesser as compared to the proposed one. Fig. 13 depicts this phenomenon in the X-Y plane. Due to the enhancement of the gain, in the X-Y plane of the proposed overall antenna, more uniform and strong intensity is observed which is shown using a dark black zone. So by this combined technique a conventional patch antenna's. gain has been enhanced by more than 7-8 dBi over the wide band.

Fig. 14 reports the simulated and measured gain for the proposed antenna. The simulated peak gain of 14.5 dBi is observed at 7.7 GHz in comparison with the measured peak gain of 13.95 dBi at 7.7 GHz. As compared to the RIS backed antenna peak gain is enhanced around 5 dB. The MM superstrate effectively increases the radiation aperture of the antenna. Hence the gain of the antenna is enhanced. It is noted that with the proposed physical size of the superstrate of 60 mm X 60 mm, maximum directivity which can be obtained, is around 15 dBi. The gain of the proposed aperture is around 14.5 dBi. So the maximum simulated aperture efficiency of around 96% is observed with this configuration.
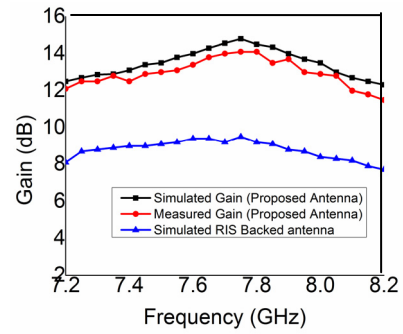

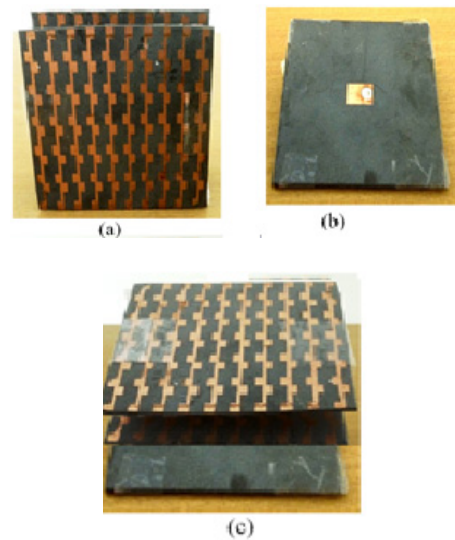**FIGURE 14.** Gain Variation over the Frequency Band.

FIGURE 15. Fabricated Prototype (a) MM Superstrate (b) RIS backed feed patch (c) fabricated prototype (d) simulated prototype.

It is also seen that with only the two layers of dielectric superstrate the gain of the antenna is increased only 1.5 dB. Fig. 15 show the photo of the fabricated prototype of the antenna and its different layer.

The drawback of this design is that it is high profile in nature but the advantage is that radiation efficiency is very high and it can be useful for high directivity application where space is not constraint over the wide bandwidth. In [3] and [6] due to the presence of the aperture coupled feed poor front to back lobe ratio is observed with radiation efficiency of 76%-86%. In [12], also due to the dielectric loss in the cavity medium obtained aperture efficiency is below 70%. In [24] and [25] the reported aperture efficiency is 70% and 83%, respectively. In [23] the enhancement in gain is observed around 7 dB, but at the same time due to the increased fabrication complexity the cross polarization is observed more. The calculated aperture efficiency in [31] is less than 60%.

The proposed configuration outperforms in terms of the calculated aperture efficiency which is obtained around 96%. Three layer based ZIML medium is also capable to produce

TABLE 2. Comparison Results with the other state of the literatures.

Ref	Size (λ^3_0)	Frequency GHz)	FBW (%)	Peak Gain (dB)	Geometry
[1]	27	9.32	----	14	Grid
[2]	8.9	8.98	----	15	Dielectric Layer
[3]	2	60	6.7	14.5	Dielectric Layer
[5]	8.9	8.34	9	18	Metal Strip Grating
[9]	40.5	14.2	< 2	19	FSS Patch array
[10]	4.5	11	5	16	EBG Multi Layer
[12]	2	10 (Multi-resonance)		12	AMC-PRS
[24]	3.81	10	< 3	16	ZIML+patch
[25]	3.2	11	< 3	10	patch + FSS
[26]	2.6	10	< 3	15	patches +MM
[31]	2.4	5.8	< 6	9	patch +holey superstrate
[PW]	**1.96**	**7.7**	**14**	**14.5**	**RIS+ patch+ ZIML**

[PW] Present Work

low refractive index over the broad band-width, which can be understood from the explanation given in the section II. It is seen that when the three layer ZIML medium is excited with the same RIS backed patch antenna, is capable to give peak gain around 16 dB over the same impedance bandwidth Finally the performance of the two layer proposed antenna has been compared with some of the already existing literatures in the Table 2 which brings out the performance improvement of the proposed structure.

V. CONCLUSION

In this paper an aperture efficient wide band directive antenna is designed using a novel multilayer based metamaterial structure combined with a Reactive Impedance Surface (RIS) backed patch antenna. The metamaterial unit cell is a two-layer structure which is stacked one after other to form the overall unit cell. This MM medium gives low refractive index over a wide bandwidth with very low loss. A RIS loaded patch antenna has been designed in the required frequency band to feed the multilayer ZIM medium. The proposed antenna gives 14% fractional bandwidth over the C and the X band. The proposed antenna enhances the peak gain of the conventional patch antenna by an amount of 8.5 dB at 8 GHz and the RIS backed patch antenna around 4-5 dB. The calculated aperture efficiency of the proposed antenna is obtained more than 96% which is higher than the conventional Resonant Cavity Antennas (RCA). Finally, the antenna has been fabricated and its performance is verified experimentally. Proposed wideband directive antenna can be useful especially where high gain is required over a wide band such as at C and X band satellite applications and space communication.

REFERENCES

[1] G. Von Trentini, "Partially reflecting sheet arrays," *IRE Trans. Antennas Propag.*, vol. 4, no. 4, pp. 666–671, Oct. 1956.

[2] X. H. Shen, P. Delmotte, and G. A. E. Vandenbosch, "Effect of superstrate on radiated field of probe fed microstrip patch antenna," *IEE Proc.-Microw., Antennas Propag.*, vol. 148, no. 3, pp. 141–146, Jun. 2001.

[3] H. Vettikalladi, O. Lafond, and M. Himdi, "High-efficient and high-gain superstrate antenna for 60-GHz indoor communication," *IEEE Antennas Wireless Propag. Lett.*, vol. 8, pp. 1422–1425, 2009.

[4] Y. Coulibaly, M. Nedil, L. Talbi, and T. A. Denidni, "High gain cylindrical dielectric resonator with superstrate for broadband millimeter-wave underground mining communications," in *Proc. 14th Int. Symp. Antenna Technol. Appl. Electromagn. Amer. Electromagn. Conf. (ANTEM-AMEREM)*, Jul. 2010, pp. 1–4.

[5] A. Foroozesh and L. Shafai, "On the characteristics of the highly directive resonant cavity antenna having metal strip grating superstrate," *IEEE Trans. Antennas Propag.*, vol. 60, no. 1, pp. 78–91, Jan. 2012.

[6] A. Pirhadi, H. Bahrami, and J. Nasri, "Wideband high directive aperture coupled microstrip antenna design by using a FSS superstrate layer," *IEEE Trans. Antennas Propag.*, vol. 60, no. 4, pp. 2101–2106, Apr. 2012.

[7] A. Agouzoul, M. Nedil, Y. Coulibaly, T. A. Denidni, I. B. Mabrouk, and L. Talbi, "Design of a high gain hybrid dielectric resonator antenna for millimeter-waves underground applications," in *Proc. IEEE Int. Symp. Antennas Propag. (APS-URSI)*, Jul. 2011, pp. 1688–1691.

[8] Y. J. Lee, J. Yeo, R. Mittra, and W. S. Park, "Application of electromagnetic bandgap (EBG) superstrates with controllable defects for a class of patch antennas as spatial angular filters," *IEEE Trans. Antennas Propag.*, vol. 53, no. 1, pp. 224–235, Jan. 2005.

[9] A. P. Feresidis, G. Goussetis, S. Wang, and J. C. Vardaxoglou, "Artificial magnetic conductor surfaces and their application to low-profile high-gain planar antennas," *IEEE Trans. Antennas Propag.*, vol. 53, no. 1, pp. 209–215, Jan. 2005.

[10] A. Pirhadi, M. Hakkak, F. Keshmiri, and R. K. Baee, "Design of compact dual band high directive electromagnetic bandgap (EBG) resonator antenna using artificial magnetic conductor," *IEEE Trans. Antennas Propag.*, vol. 55, no. 6, pp. 1682–1690, Jun. 2007.

[11] H. Attia, L. Yousefi, and O. M. Ramahi, "Analytical model for calculating the radiation field of microstrip antennas with artificial magnetic super-strates: Theory and experiment," *IEEE Trans. Antennas Propag.*, vol. 59, no. 5, pp. 1438–1445, May 2011.

[12] Y. Sun, Z. N. Chen, Y. Zhang, H. Chen, and T. S. P. See, "Sub-wavelength substrate-integrated Fabry–Pérot cavity antennas using artificial magnetic conductor," *IEEE Trans. Antennas Propag.*, vol. 60, no. 1, pp. 30–35, Jan. 2012.

[13] Y. H. Liu and X. P. Zhao, "Investigation of anisotropic negative permeability medium cover for patch antenna," *IET Microw., Antennas Propag.*, vol. 2, no. 7, pp. 737–744, Oct. 2008.

[14] B. Majumder, K. Kandasamy, J. Mukherjee, and K. P. Ray, "A high gain EBG backed slot antenna loaded with anisotropic mu-negative super-strate," in *Proc. IEEE Int. Symp. Antennas Propag. USNC/URSI Nat. Radio Sci. Meeting*, Jul. 2015, pp. 476–477.

[15] B. Majumder, K. Kandasamy, J. Mukherjee, and K. P. Ray, "A compact broadband directive slot antenna loaded with cavities and single and double layers of metasurfaces," *IEEE Trans. Antennas Propag.*, vol. 60, no. 4, pp. 2101–2106, Apr. 2012.

[16] D. Mitra, B. Ghosh, A. Sarkhel, and S. R. B. Chaudhuri, "A miniaturized ring slot antenna design with enhanced radiation characteristics," *IEEE Trans. Antennas Propag.*, vol. 64, no. 1, pp. 300–305, Jan. 2016.

[17] M. Silveirinha and N. Engheta, "Tunneling of electromagnetic energy through sub-wavelength channels and bends using ε-near-zero materials," *Phys. Rev. Lett.*, vol. 97, Oct. 2006, Art. no. 157403.

[18] F. Bilotti, S. Tricarico, and L. Vegni, "Plasmonic metamaterial cloaking at optical frequencies," *IEEE Trans. Nanotechnol.*, vol. 9, no. 1, pp. 55–61, Jan. 2010.

[19] H. Zhou *et al.*, "A novel high-directivity microstrip patch antenna based on zero-index metamaterial," *IEEE Antennas Wireless Propag. Lett.*, vol. 8, pp. 538–541, 2009.

[20] S. Enoch, G. Tayeb, P. Sabouroux, N. Guérin, and P. Vincent, "A metamaterial for directive emission," *Phys. Rev. Lett.*, vol. 89, no. 21, p. 213902, 2002.

[21] B.-I. Wu, W. Wang, J. Pacheco, X. Chen, T. M. Grzegorczyk, and J. A. Kong, "A study of using metamaterials as antenna substrate to enhance gain," *Prog. Electromagn. Res.*, vol. 51, pp. 295–328, 2005.

[22] F.-Y. Meng, Y.-L. Lyu, K. Zhang, Q. Wu, and J. L.-W. Li, "A detached zero index metamaterial lens for antenna gain enhancement," *Prog. Electromagn. Res.*, vol. 132, pp. 463–478, 2012.

[23] P. Q. Turpin Wu, D. H. Werner, B. Martin, M. Bray, and E. Lier, "Near-zero-index metamaterial lens combined with AMC metasurface for high-directivity low-profile antennas," *IEEE Trans. Antennas Propag.*, vol. 62, no. 4, pp. 1928–1936, Apr. 2014.

[24] D. Li, Z. Szabo, X. Qing, E.-P. Li, and Z. N. Chen, "A high gain antenna with an optimized metamaterial inspired superstrate," *IEEE Trans. Antennas Propag.*, vol. 60, no. 12, pp. 6018–6023, Dec. 2012.

[25] L. Kurra, M. P. Abegaonkar, A. Basu, and S. K. Koul, "FSS properties of a uniplanar EBG and its application in directivity enhancement of a microstrip antenna," *IEEE Antennas Wireless Propag. Lett.*, vol. 15, pp. 1606–1609, 2016.

[26] K. A. Singh, P. M. Abegaonkar, and S. K. Koul, "High-gain and high-aperture-efficiency cavity resonator antenna using metamaterial superstrate," *IEEE Antennas Wireless Propag. Lett.*, vol. 16, pp. 2388–2391, 2017.

[27] Computer Simulation Technology GmbH. (2012). *CST Microwave Studio*, Framingham, MA, USA. [Online]. Available: https://www.cst.com/

[28] J. B. Pendry, A. J. Holden, W. J. Stewart, and I. Youngs, "Extremely low frequency plasmons in metallic mesostructures," *Phys. Rev. Lett.*, vol. 76, no. 25, pp. 4773–4776, Jun. 1996.

[29] J. B. Pendry, A. J. Holden, D. J. Robbins, and W. J. Stewart, "Low frequency plasmons in thin wire structures," *J. Phys., Condens. Matter*, vol. 10, no. 22, pp. 4785–4809, 1998.

[30] Z. Szabo, G.-H. Park, R. Hedge, and E.-P. Li, "A unique extraction of metamaterial parameters based on Kramers–Kronig Relationship," *IEEE Trans. Microw. Theory Techn.*, vol. 58, no. 10, pp. 2646–2653, Oct. 2010.

[31] J. H. Kim, C. H. Ahn, and J. K. Bang, "Antenna gain enhancement using a holey superstrate," *IEEE Trans. Antennas Propag.*, vol. 64, no. 3, pp. 1164–1167, Mar. 2016.

BASUDEV MAJUMDER was born in Kolkata, India. He received the B.Tech. degree in electronics and communication engineering from the West Bengal University of Technology, Kolkata, in 2009, the M.E. degree in nuclear engineering from the School of Nuclear Studies and Application, Jadavpur University, Kolkata, in 2011, and the Ph.D. degree in electrical engineering (RF and microwave) from IIT Bombay, Mumbai, India, in 2017. He is currently an Assistant Professor with the Department of Avionics, Indian Institute of Space Science and Technology, Department of Space, Government of India. His current research interests include RF and microwave devices, metamaterial-based antennas, and microstrip antennas.

KRISHNAMOORTHY KANDASAMY received the B.E. degree in electronics and communication engineering from Bharathiar University, Coimbatore, India, in 2003, the M.E. degree in communication systems from the College of Engineering, Guindy, Anna University, Chennai, India, in 2007, and the Ph.D. degree in electrical engineering from IIT Bombay, Mumbai, India, in 2016. He is currently an Assistant Professor with the Department of Electronics and Communication Engineering, National Institute of Technology Karnataka, Surathkal, India. His current research interests include metamaterials, antenna engineering, microwave integrated circuits (MICs), and monolithic MICs.

KAMLA PRASAN RAY (M'93–SM'04) received the M.Tech. degree in microwave electronics from the University of Delhi and the Ph.D. degree from the Department of Electrical Engineering, IIT Bombay. In 1985, he joined SAMEER, TIFR, Mumbai, as the Programme Director, where he was involved in RF and microwave systems/components and developed expertise in the design of antenna elements/arrays and high-power RF/microwave sources for RADAR and industrial applications. He was a Guest/Invited/Adjunct Faculty Member with the Department of Electrical Engineering, IIT Bombay, the University of Mumbai, and CEERI (CSIR), Pilani for Postgraduate Courses. He is currently a Professor and the Head of the Department of Electronics Engineering, Defense Institute of Advanced Technology, Pune. He has co-authored a book under the supervision of Prof G. Kumar for Artech House, USA, and published over 330 research papers in international/national journals and conference proceedings. He holds three patents and filed three patents. He has successfully executed over 46 projects sponsored by Government agencies/industries in the capacity of a designer, a chief investigator, and a project manager.. He is a fellow of IETE and a Life Member of the Instrument Society of India and Engineers of EMI/EMC Society of India. He has been in advisory capacity for many international/national conferences, engineering colleges, chaired many sessions, and delivered several invited talks. He is an Associate Editor of the *International Journal on RF and Microwave Computer-Aided Engineering* (John Wiley) and a Reviewer of the IEEE TAP, AWPS, IET (Formerly IEE, U.K.), the *International Journal of Antennas and Propagation* (USA), PIERS (USA), the *International Journal of electronics* (USA), the *Journal of Electromagnetic Waves and Applications* (USA), the *International Journal of Microwave and Optical Technology* (USA), the *International Journal of Microwave Science and Technology* (Hindwai), AEU (Elsevier), SADHNA (Springer), IETE (India), and many international/national conferences and chaired many sessions.

● ● ●